A New Numerical Approach for Rotorcraft Aerodynamics Using Vorticity Confinement

Clin M. Wang*
Flow Analysis, Inc.
Tullahoma, TN

John S. Steinhoff**
University of Tennessee Space Institute
Tullahoma, TN

and

Paul M. Stremel†
NASA Ames Research Center
Moffett Field, CA

Abstract

The Vorticity Confinement method is used in conjuction with uniform Cartesian grids for computing flows of blunt bodies. These bodies are defined on the uniform grid by a smooth function where the function is designated zero on the body surfaces. A unique computation procedure is applied to all the grid points with the confinement performed outside the body based on the vorticity whereas inside the body based on the function. For flows around streamline-like bodies, such as a wing, the computation is performed on body-fitted grids where these grids can be encompassed by the uniform grid. Flow informations are transferred between the body-fitted grids and the uniform grid, where one or more blunt bodies are embedded, through an overset grid technique. However, there is no hole-cutting needed since the solid bodies are explicitly defined by the smooth function. A NACA0012 wing download under a rotor is computed by the combined approach with a generic nacelle at the wing tip.

Introduction

The complexity of flowfields around rotorcraft and the lack of efficient numerical procedures to analyze these flows make the prediction of rotorcraft aerodynamics very difficult and inadequate. This is mainly due to the fact that the flow is highly unsteady and strong, concentrated vortices are shed from rotor blades. The proximity and the persistence of these vortices generate effects that are not negligible on many aspects of the rotorcraft aerodynamics. Problems involving the strong vortices shed by the rotor blades are blade-vortex interactions, wing download under a rotor, and helicopter rotor-fuselage interactions.

Because of the importance of the vortex-dominated flows, many researchers have attempted to find viable numerical methods for these flow predictions over the past decades. In spite of these efforts, accurate and efficient methods that are suitable for rotorcraft aerodynamic analysis still do not exist. Limited success is achieved in the past for the Eulerian approach using high order discretization schemes and fine regular grids for the study of a vortex impinging on an airfoil [1]. Adaptive grid schemes are also used for a vortex impinging on an airfoil [2], a steady vortex shed at the tip of a straight wing [3], and a vortex sheet shed from the leading-edge of a delta wing [4]. It can be shown that these Eulerian approaches require a lot of computer resources, and despite the fine grids used and the adaptive embedding of extra grid points in the vortical region, these methods

* Senior Scientist, Member AIAA
** Professor, Member AIAA
† Aerospace Engineer

apparently still are not able to compute the shed vortex without having it spread over a region much larger than measured in experiments.

An other approach, The Lagrangian approach, uses ad hoc structures for vortices without resorting to a detailed, high-resolution Navier-Stokes solver. This is made of the fact that the internal structure of vortical regions, such as vortex sheets, are not important since the dimensions of these structures are small compared to other dimensions of the problem. As long as the centroid surfaces of these vortex sheets are accurately computed, together with the total vorticity surrounding each point on the centroid surface, the overall flow solution is acceptable. Some of the most efficient methods for treating the thin vortical flows currently involve Lagrangian marker-based schemes, where vorticity or circulation is assigned to individual markers which convect through the flowfield. These methods, in the form of "Vortex Lattice" or "Vortex Blob" techniques for incompressible flows [5] and "Vortex Embedding" techniques for compressible flows [6], entail representation of vortex sheets or vortex filaments by surfaces or lines defined by markers. The disadvantage to these Lagrangian methods is that the topology of each vortical region should be known beforehand so that suitable arrays of markers can be computationally defined. In addition, the vortical regions may interact with solid surfaces and their topology may change. This requires new specifications of the markers and re-connection.

The computational technique used here is fundamentally different from the previously described methods in that it involves adding a term to the continuum flow equations before discretization, and therefore modifies the basic Euler/Navier-Stokes equations. With the added term, the flow equations admit solutions with concentrated vortices that can convect without spreading, even if the basic equations have diffusive terms. For this reason, simple, low order diffusive numerical schemes can be used to discretize and solve the modified flow equations without resulting in vortices that spread as they convect. The present approach is similar to shock capturing where the detailed internal dynamics of shocks are not computed, but rather a modified set of equations is solved which results in a shock spread over a few number of grid cells. The resulting internal structure satisfies conservation laws in integral form.

The present Vorticity Confinement method was used to compute rotorcraft aerodynamics involving single component using moderate coarse grids of body-fitted topology. These include a 2D airfoil dynamic stall and a vortex ring over a circular cylinder [7], a 3D wing dynamic stall [8], and a download study of a 3D isolated wing [9]. These results have been compared well with 2D experimental and other numerical results. Extensive comparisons of the 3D wing dynamic stall results were made with the available wind tunnel test results [10]. It is shown that the numerical results compare well with the test data considering the experimental error bounds. With the present approach, the results of these streamline-like bodies using the body-fitted grids demonstrate the method is robust and the numerical diffusion is effectively eliminated using coarse grids.

For a blunt body with complex geometry, such as a helicopter fuselage, it is usually difficult, if not impossible, to robustly generate a body-fitted grid around the body. The effect of the presence of such a body in the flowfield often cannot be ignored. With the Vorticity Confinement, blunt bodies can be studied robustly using a uniform Cartesian grid. This is achieved by defining a smooth function on the uniform grid. On the body surface, the function is assigned to be zero, where the function is positive outside the body and negative inside the body. With the definition of the function on the uniform grid, the body geometry is explicitly defined and no other specific boundary conditions on the body surfaces are required during the computation. One or more blunt bodies can be intrinsically defined by a smooth function.

The uniform Cartesian grid, together with the Vorticity Confinement method, offers a great advantage for the computation of rotor-body interaction problems. The uniform grid not only contains one or more blunt bodies but also serves as a background grid where additional body-fitted grids wrapped around streamline-like rotor blades are encompassed by the uniform grid. Flow information between the uniform grid and the body-fitted grids are transferred through an overset grid technique. This allows the computation of a complex rotor-body interation problem to become a much simpler task, compared to a computation that uses also additional body-fitted grid for blunt bodies. Moderate coarse grids are allowed to be used by the present procedure without resulting in excessive numerical diffusion. In adition, the procedure can be used in the future for parametric study and design purposes. In this study, a wing download under a rotor and with the appearance of a generic nacelle is computed using the combined approach. The nacelle is treated as a blunt body embedded within the uniform grid.

Numerical Method

The Vortocity Confinement method is developed primarily for eliminating the numerical diffusion. Any conventional method that uses finite discretization schemes will inevitably inherent the numerical diffusion. For complicated flows, the grid used can not be fine everywhere for the whole computational domain. To achieve a highly efficient procedure that can be used for parametric study and design purposes, a method must be robust and perform well on coarse grid. That is, coarse grids can be used without generating appreciable numerical diffusion. This feature is particularly important for rotorcraft aerodynamics studies since concentrated vortices are present for most of the flow domain and their effects cannot be ignored even in the far wake from the rotor.

The method developed and used here involves adding a term to the momentum part of the continuum Euler/Navier-Stokes equations. The extra "Confinement" term is local and simple to discretize. It is non-zero only within the vortical regions and does not change the total vorticity or mass within those regions. The technique is applicable to general compressible and incompressible flows. Here, the Vorticity Confinement method is described for incompressible flow using the velocity-pressure formulation. For a general unsteady flow,

$$\nabla \cdot \vec{q} = 0 \tag{1}$$

$$\partial_t \vec{q} = -(\vec{q} \cdot \nabla)\vec{q} + \nabla p/\rho + \nu \nabla^2 \vec{q} + \epsilon \vec{s} \tag{2}$$

where $\vec{q}$ is the velocity vector; t is time; p, ρ, and ν represent pressure, density, and the diffusion coefficient, respectively. The additional term, $\epsilon\vec{s}$, is the "Confinement" term where the numerical coefficient ϵ controls the size of the convecting vortical regions. The confinement term has the form:

$$\vec{s} = -\vec{n} \times \vec{\omega} \tag{3}$$

$$\vec{n} = \nabla\eta/|\nabla\eta| \tag{4}$$

where

$$\vec{\omega} = \nabla \times \vec{q} \tag{5}$$

is the vorticity vector and η is a scalar field that has a local minimum on the centroid of the vortical region:

$$\eta = -|\vec{\omega}| \tag{6}$$

For the confinement term, expressed by Eq. (3), $\vec{n}$ in the equation is a unit vector pointing toward the centroid of the vortical region and the term serves to convect $\vec{\omega}$ back toward the centroid as $\vec{\omega}$ diffuses away. This convection increases the diffusion and a steady-state form results when the two terms become balanced. It is noted that steady-state solutions exist, for any positive value of ϵ. It appears to be better to discretize the set of Eqs. (1) and (2) for problems which have thin, well-behaved vorticity distribution, even in the presence of the numerical diffusion, than to discretize the un-modified equations which only admit vorticity regions that continue to spread, if there is any numerical diffusion.

An important feature of the vorticity confinement method is that the velocity correction is limited to the vortical region only. The correction effectively convects vorticity back towards the local extreme of the vortical region. The total change induced by the confinement term in mass, δI_ρ, and vorticity, δI_ω, can be expressed by

$$\delta I_\rho = \epsilon \int_{R_\omega} \nabla \cdot \vec{s} dV \tag{7}$$

$$\delta I_\omega = \epsilon \int_{R_\omega} \nabla \times \vec{s} dV \tag{8}$$

The integration is performed on the vortical domain, R_ω. It is simple to show that $\delta I_\rho = 0$ and $\delta I_\omega = 0$ by using Eq. (3), i.e., the confinement term conserves the mass and the total vorticity. Conservation properties involving fluid momentum are discussed in Refs. 11 and 12.

Numerical Implementation

The Vorticity Confinement method is easy to implement on any conventional Navier-Stokes/Euler solver, incompressible or compressible. For the present work, the method is implemented to a basic procedure that uses a velocity-split procedure [13] for solving general vortex-dominant incompressible flows. The basic procedure is for the solution of Navier-Stokes/Euler equations and it is used for both body-fitted grids and uniform Cartesian grids. For any new time level, the velocity solution is sought by the following three steps knowing the velocity at an old time level. The three steps are:

1. A finite-difference form of the following equation is solved,

$$\vec{q}^{\,*} = \Delta t[\vec{q}^{\,n} - (\vec{q}^{\,n} \cdot \nabla)\vec{q}^{\,n} + \nu\nabla^2\vec{q}^{\,n}] \tag{9}$$

   where $\vec{q}^{\,*}$ denotes an intermediate velocity at the new time level, by convection and diffusion after a time step Δt. The velocity field $\vec{q}^{\,n}$ is the known, existing velocity field at the old time level n. The convection term is discretized by a second upwind differencing [14] whereas the diffusion term is discretized by a central differencing. On a body-fitted grid, the contravariant velocity is discretized and the computation is performed on the transformed space. On a uniform Cartesian grid, the discretization is simple and the computation is performed directly on the physical space.

2. A Poisson equation derived from the continuity equation is solved,

$$\nabla^2 \phi = -\nabla \cdot \vec{q}^* \tag{10}$$

where the potential ϕ is solved by a multi-grid relaxation technique. The obtained velocity $\vec{q}^*$ from Step 1 is corrected if the right side of Eq. (10) is not zero, indicating a violation of the mass conservation. The multi-grid procedure is greatly simplified for a Cartesian grid computation.

3. The corrected velocity field for the new time level is

$$\vec{q}^{n+1} = \vec{q}^* + \nabla \phi \tag{11}$$

where $\vec{q}^{n+1}$ denotes the velocity at the new time level. The pressure can be obtained by the potential field if the pressure is desired.

The above three steps constitute the basic computational loop to advance the velocity field from an old time level to a new time level. The vorticity field, obtained by the differentiation of the velocity field, exhibits ever-spreading characteristics as time progresses.

To achieve a solution that offsets the numerical diffusion, the Confinement term, $\epsilon\vec{s}$ in Eq. (2), is computed after the Step 1 is performed. With the computed known velocity $\vec{q}^*$, the vorticity field is first computed. The directional unit vector $\vec{n}$ and therefore the confinement velocity $\vec{s}$ are determined by Eqs. (3)-(6). The velocity field after the confinement modification is then

$$\vec{q}^C = \vec{q}^* + \epsilon\vec{s} \tag{12}$$

The added confinement velocity term has the effect to transport the vorticity back toward its local maximum against the direction of numerical diffusion, that always exists for a discretized computation. The velocity $\vec{q}^C$ carries a vorticity field that is confined in thinner regions compared with the vorticity carried by the velocity field $\vec{q}^*$.

With the modified velocity field $\vec{q}^C$, the Steps 2 and 3 are performed where $\vec{q}^*$ in Eqs. (10) and (11) is replaced by $\vec{q}^C$. Notice that the two steps do not change the vorticity distribution. Therefore, the vorticty carried by the velocity for the new time level, $\vec{q}^{n+1}$, has the same distribution as that carried by the velocity field $\vec{q}^C$. Adding the confinement velocity results in a vorticity that confines to thin regions. With this procedure, coarse grids are allowed to be used.

The Vorticity Confinement method not only can be used to get velocity that has the confined vorticity field, but can also be used for general blunt bodies when a body is defined in a simple uniform Cartesian grid. A smooth function F or its value can be determined for almost any blunt body geometry. On the body surface, F is defined zero. Inside the body surface, F is negative and its value is decreasing away from the surface. Outside the body surface, F is positive. This smooth function defined at each grid point uniquely describes a blunt body. The confinement procedure described earlier can be applied to the whole uniform grid, inside and outside the solid body, except two more steps are taken for the region inside the body.

For regions inside solid bodies, first, the known velocity at any time level is multiplied by a factor $1/|1-F|$. This is to ensure the velocity inside the body is ever-diminishing, but gradually. The velocity field is then added a velocity modification, $\epsilon\vec{s}$ shown in Eq. (2). Here, the unit normal direction in Eq. (4), however, has a different form:

$$\vec{n} = \nabla F / |\nabla F| \tag{13}$$

The adding of the confinement velocity vector inside the body has a different effect compared to the region outside the body. While outside the body, the correction of the velocity is to transport the vorticity back toward local maximum, the correction performed inside the body virtually transport the vorticity toward the body surface. With the two additional steps performed at each time step for the grid points inside the body, the velocity goes to zero as the time progresses and the vorticity is correctly distributed to the body surface. Notice the mass balance inside and outside the blunt bodies is ensured by the Steps 2 and 3.

The ability to use the uniform grid offers a simple and yet effective way to treat rotorcraft rotor-body interaction problems. For a helicopter problem, the fuselage geometry can be described by a function F and the fuselage is defined uniquely in the uniform grid. No additional definition of the body geometry is needed. The uniform grid also serves as a background grid where rotor solution obtained by a rotor solver is transferred to the uniform grid and transported by the grid. This transfer only takes a simple interpolation. The whole domain of the uniform grid is computed by the procedure described as above, with velocity confinement term differently computed inside and outside the body surface depending on the sign of F.

For a wing download study with a rotor and a nacelle, the nacelle can be treated as a blunt body and is defined by a function F on the uniform grid. The body-fitted grid around the wing can be treated as an additional domain embedded in the uniform grid where the two grids are transferring information through an overset-grid technique. However, no hole-cut is needed as required by a conventional overset-grid technique. This is because the function F already defines the location of the solid surface, and inside the surface, flow is computed simultaneously using the Vorticity Confinement method. Detailed flow near the wing is computed by the body-fitted grid wrapped around the wing. In addition, a rotor wake is transferred to the uniform grid from a rotor solution as the wake vortices also are convected in the uniform grid. In this case, the uniform grid not only serves as a background grid, but also includes a nacelle as a blunt body embedded. Flow solution near the wing therefore contains the effect of the presence of the nacelle and the rotor wake.

Results and Discussions

The numerical procedure is used to compute flows of a helicopter with a rotor and a wing download with a generic nacelle and a rotor. In this paper, only the wing download study is presented. Helicopter results were included in Ref. 15 where a combination of an Apache rotor and fuselage was computed. For the wing download study, an isolated wing without a nacelle and a rotor was computed and documented in Ref. 9 using a body-fitted grid. The wing computed was a NACA0012 wing of rectangular planform and has a half-span aspect ratio of 2.55, with a rounded tip. Without the influence of a rotor wake, the wing is under a constant angle of attack of -90^o. A vortex ring, which simulates a rotor wake, was added into the body-fitted grid used for the isolated wing.

Figures 1 and 2 are drawn from Ref. 9 and show the surface pressure for the isolated wing without the influence of the vortex ring. The base pressure as well as the stagnation pressure on the upper surface demonstrate a trend of decreasing from the root toward the tip. This is because of the flow expansion across the wing tip. Figure 3, also drawn from Ref. 9, shows the surface pressure of the same wing with the influence of a vortex ring passing from above the wing. The effect of the passage of the ring is clearly seen by the localization of a maximun pressure at the upper surface at $T = 1.2$ and $T = 5.2$. At a much later time, $T = 10.9$, where the ring already passes the wing, the surface pressure recovers to a distribution of the un-disturbed wing shown in Fig. 2.

A uniform Cartesian grid is then used to include an ellipsoid as a generic nacelle located at the wing tip. A body fitted grid is encompassed by the uniform grid, where the body-fitted grid covers the wing span and the wing tip is flat. Figure 4 demonstrates the geometry and the relative locations of the wing, the wing and the generic nacelle, and the wing and the nacelle and a three-blade rotor that will be computed later.

A generic nacelle, represented by an ellipsoid here, is embedded in a uniform Cartesian grid. The function F which defines the ellipsoid can be expressed analytically:

$$F = a(y - y_0)^2 + b[(x - x_0)^2 + (z - z_0)^2] - r^2 \qquad (14)$$

where the main axis is parallel to the y-axis, a b c and r are constants defining the ellipsoid geometry, and (x_0, y_0, z_0) is the ellipsoid center. The ellipsoid surface is defined by $F = 0$. On the uniform grid, F is known at every point, positive outside the ellipsoid surface and negative inside the ellipsoid. A grid of $65 \times 65 \times 65$ with a grid size of 0.08 (the wing chord is of unit length) is used here. A body-fitted O-grid wrapped around the flat-tip wing, of a size $65 \times 17 \times 17$, is used where the three numbers denote grid numbers in circumferential, normal, and spanwise directions.

Using the combined approach, the ellipsoid is first absent from the uniform grid, that is, F is set to 1 for every grid point. Flow solution of the body-fitted grid is mapped to the uniform grid where the region overlaps with the body-fitted grid. With newly computed flow for the uniform grid, the outer boundary of the body-fitted grid is obtained by interpolation from the uniform grid. Computed surface pressure for the wing is shown in Fig. 5. The pressure distribution for the three spanwise stations exhibit a similar pattern as that of the wing-alone calculation using only the body-fitted grid, shown in Fig. 1. The difference is attributable mainly to the difference of the tip geometry for the two cases. Both the cases are for a wing of the half span aspect ratio of 2.55.

With the nacelle present, the pressure distribution is shown in Fig. 6. It is seen that the base pressure of the three spanwise stations sits almost at the same level, approximately 0.5. The presence of the nacelle prevents the flow expansion from the upper surface toward the lower surface and therefore the base pressure is nearly identical.

Finally, a three blade rotor is included and placed above the generic nacelle. The rotor blade is of a cross section of NACA 0020 at the root region and NACA 0015 at the tip region, without twist and taper. This blade geometry has been tested by the Army Lab in Moffett Field, CA for a two-blade rotor [16]. The complete assembly of the grid including a body-fitted wing grid, the uniform grid containing the nacelle, and the three-blade rotor is shown in Fig. 7.

The three blade rotor solution is obtained by the HELIX code [17] for hover condition. The HELIX code is based on a vorticity embedding method and is a compressible, full potential flow solver. Since the flow is periodic, solution for only one blade is required. The rotor solution is obtained on a body-fitted H-grid with periodic boundary condition imposed on both the upstream and the downstream boundaries. Figure 8 shows the computed velocity field at a plane about one chord downstream of the rotor blade. Figure 9 is the vorticity contours for the same plane. The first passage tip vortex is clearly defined by the vorticity contours just below the rotor disk, whereas the other earlier shed tip vortices are smeared due to the coarse grid away from the rotor disk. The grid of the plane is shown in Fig. 10 together with the grid in the disk plane. This grid is also contained by the background uniform Cartesian grid.

The rotor solution obtained by the HELIX code is first fed into the uniform grid, where the nacelle and the wing are absent. Initially, the whole rotor solution is interpolated to the uniform grid to start as an initial velocity field. Later, at each time step, the HELIX solution rotates an angle of $\Omega \times \Delta t$, where Ω is the blade rotational speed, and only a segment of the HELIX solution behind each blade is interpolated onto the uniform grid. A segment of the tip vortex is therefore transferred to the uniform grid and, once there, is transported inside the uniform grid. Vorticity iso-surfaces shown in Fig. 11 show the wake of the three-blade rotor after 2 revolutions. The vortex structure is preserved by the Vorticity Confinement method. A uniform downflow is added to the computation to accelerate the downward movement of the tip vortices.

Once the rotor wake is established in the uniform grid, the nacelle is put into the uniform grid and the body-fitted grid of the wing is included in the solution procedure. Figure 12 shows the vortex wake of the complete geometry, where the vortex is represented by an iso-surface of the vorticity magnitude. A uniform downflow is added and therefore the solution simulates a climbing state. Vorticity shed by the rotor, the wing, and the nacelle are seen in the figure. The shade of the wing surface and the ellipsoid shown here represents the surface pressure. Figure 13 shows the surface pressure of the wing for three spanwise stations. The base pressure, which is almost at the same level in the previous wing plus nacelle calculation, exhibits a mild variation due to the presence of the rotor wake. Figure 14 shows the pressure contours on the wing upper and the lower surfaces. On the upper surface, the compression due to the passing vortices is clear, which is qualitatively similar to the surface pressure of a passing vortex ring, shown in Fig. 3.

The wing-nacelle-rotor computation takes about 20 CPU seconds for each time step running on a CRAY C90 computer. Each revolution of the rotor blade takes 60 steps to complete in this computation and therefore for each revolution, it takes approximately 20 minutes of the CRAY CPU time. In this computation, the uniform Cartesian grid is of a size of $97 \times 65 \times 97$, where the second number is in the up-down direction.

Concluding Remarks

The present study demonstrates that the Vorticity Confinement method and the use of a uniform Cartesian grid are ideal for computing complicated rotorcraft aerodynamic interaction problems. This method allows using coarse grids and low-order differencing schemes where the numerical diffusion is effectively eliminated. To the author's knowledge, the method is the most effective and, probably, the only one currently available that is economic and also fairly accurate for solving the rotorcraft aerodynamics. The present approach, furthermore, can be used as a tool in the future for parametric study and design purposes.

The most important contributing factors for the present method are the implementation of the Vorticity Confinement and the ability to use the uniform Cartesian grid. The combined computation using the Cartesian grid and body-fitted grid allows the computation of complex body rotor interactions becomes a much simpler task. Major features, such as transport of concentrated vortices and vortex shedding from the blunt body, are computed with success. The transfer of information between the Cartesian grid and the body-fitted grid is simple and straight. No hole-cutting is needed because the function F carries all the body information.

In the present uniform Cartesian grid computation for the blunt body, however, the details of the flow near the surface are not computed. This is because the uniform grid used in general is not conformed with the body surface and boundary layers attached to the surface are represented by a vortex sheet within a few grid cells.

For the wing download studied here, the rotor solution from HELIX code is treated as a fixed solution and the solution itself does not feel the presence of the wing presented downstream of the rotor disk. It is therefore that only one-direction interference is accomplished. The mutual interaction of the rotor-wing problem can be studied by solving the flow near the rotor blade every time step or every several steps. A solver that performs well for the blade, such as TURNS code [18], is ideal to be integrated into the solution procedure.

References

1. Rai, M. M., "Navier-Stokes Simulations of Blade-Vortex Interaction Using High Order Accurate Upwind Schemes," AIAA Paper No. 87-0543, 1987.
2. Oden, J. T., Strouboulis, T. and Devloo, P., "Moving-Grid Finite Element Algorithm for Supersonic Flow Interaction Between Moving Bodies," *Computational Methods in Applied Mechanical Engineering*, Vol. 59, 1986.
3. Strawn, R. C.,"Wing Tip Vortex Calculation with an Unstructured Adaptive Grid Euler Solver," presented at the *47th AHS Forum of the American Helicopter Society*, 1991.
4. Moore, D. W., "A Numerical Study of the Roll-Up of a Finite Vortex Sheet," *Journal of Fluid Mechanics*, Vol. 63, 1974.
5. Hoeijmakers, W. M. and Vaatstra, W., "A Higher Order Panel Method Applied to Vortex Sheet Roll-Up," *AIAA Journal*, Vol. 21, 1983.
6. Steinhoff, J. S., and Ramachandran, K., "A Vortex Embedding Method for Free-Wake Analysis of Helicopter Rotor Blades in Hover," *Vertica*, Vol. 13, 1989.
7. Wang, C. M., Steinhoff, J. S. and Wenren, Y., "Numerical Vorticity Confinement for Vortex-Solid Body Interaction Problems," *AIAA Journal*, Vol. 33, 1995.
8. Wang, C. M. and Stremel, P. M., "Numerical Study of Stall of Oscillating Wings," AIAA Paper 96-2490, 1996.
9. Wang, C. M. and Stremel P. M., "Numerical Study of Wing Download," AIAA Paper 96-0674, 1996.
10. Piziali, R. A., "2D and 3D Oscillating Wing Aerodynamics for a Range of Angles of Attack Including Stall," NASA TM-4632, 1994.
11. Steinhoff, J. S., Wenren, Y., Mersch, T., and Senge, H., "Computational Vorticity Capturing: Application to Helicopter Rotor Flow," AIAA Paper No. 92-0056, 1992.
12. Steinhoff, J. S., Thomas, M. and Wenren, Y., "Computational Vorticity Confinement: Two Dimensional Incompressible Flow," SECTAM XVI Conference, 1992.
13. Kim, J. and Moin, P., "Application of a Fractional-Step Method to Incompressible Navier-Stokes Equations," *Journal of Computational Physics*, Vol. 59, 1985.
14. Roach, P. J., *Computaional Fluid Dynamics*, Hermosa Publishers, New Mexico, 1976.
15. Wang, C. M. and Wenern, Y., "A Unified Numerical Approach for Rotorcraft Aerodynamics," Final Report, NASA SBIR II Contract NAS2-14205, 1997.
16. McAlister, K. W., Schuler, C. A., Branum, L. and Wu, J. C., "3-D Wake Measurements Near a Hovering Rotor for Determining Profile and Induced Drag," NASA TP-3357, 1995.
17. Ramachamdran, K., Schlechtriem, S. Caradonna, F. X. and Steinhoff, J. S., "The Application of Vorticity Embedding to the Computation of Advancing Rotor Flows," the AHS 49th Annual Forum, 1993.
18. Srinivasan, G. R., Baeder, J. D., Obayashi, S. and McCroskey, W. J., " Flowfield of a Lifting Hovering Rotor - A Navier-Stokes Simulation," NASA TM-102862, 1990.

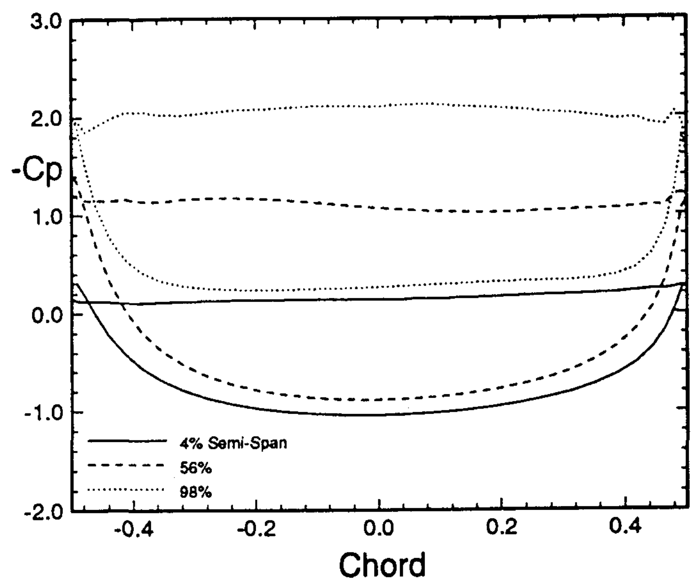

Figure 1. Pressure Distribution, Half-Span Aspect Ratio 2.55

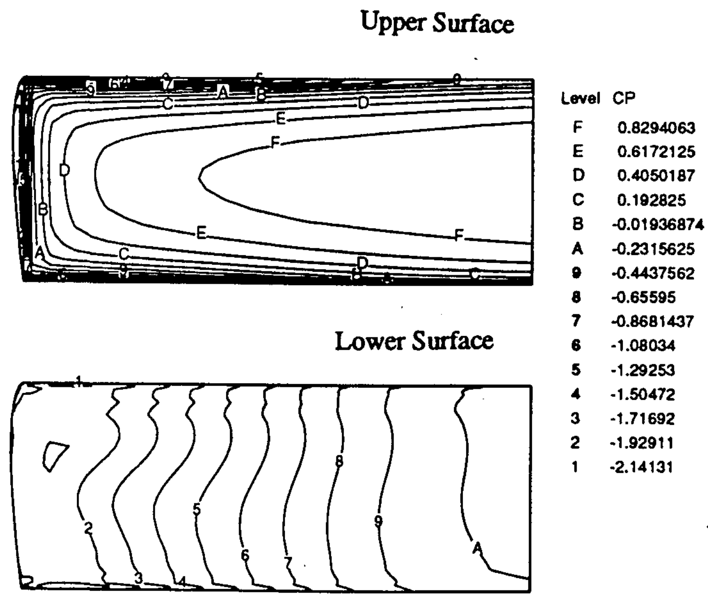

Figure 2. Pressure Contours, Half-Span Aspect Ratio 2.55

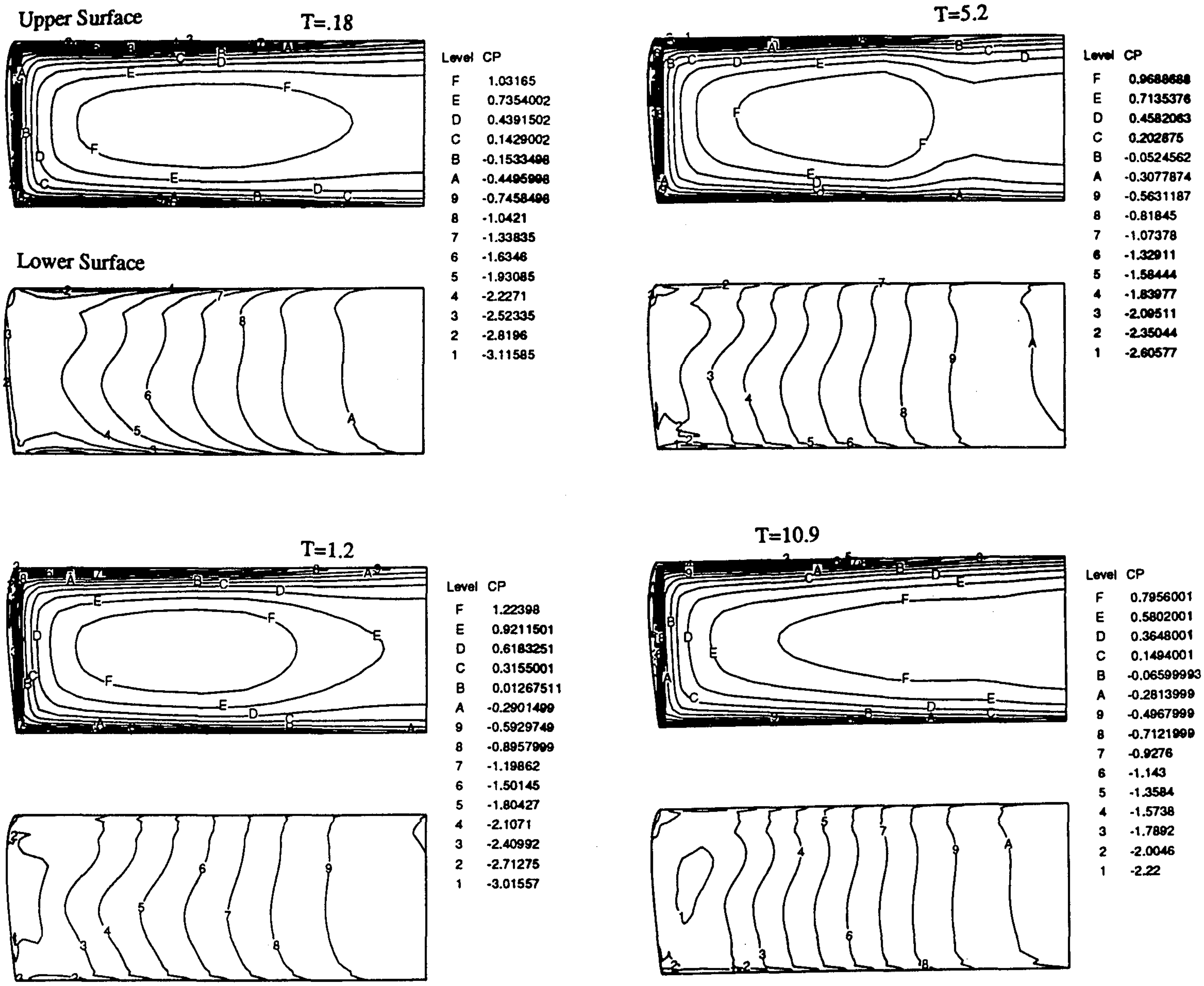

Figure 3. Time Variation of Surface Pressure Contours, with Vortex Ring

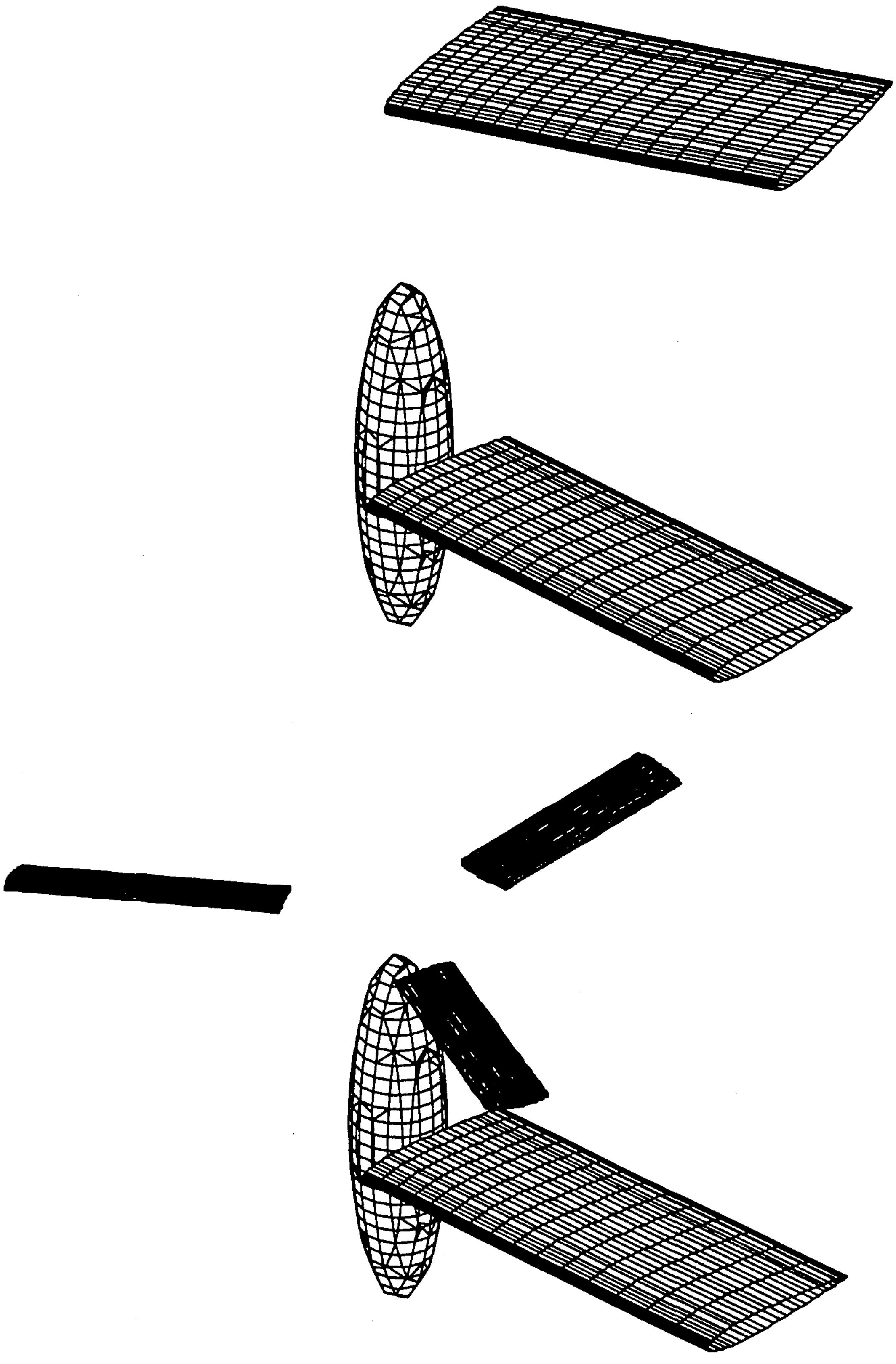

Figure 4. Geometries Studied for Wing Download

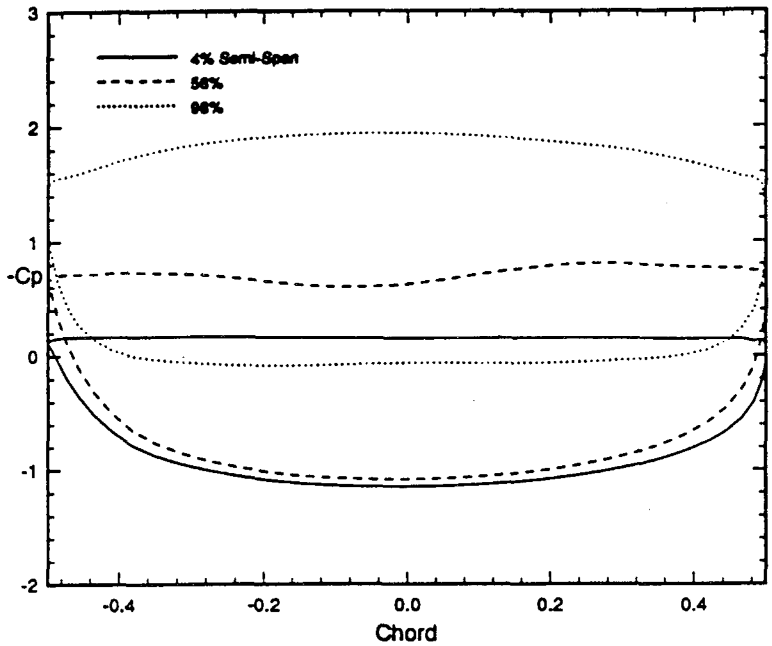

Figure 5. Pressure Distribution, Combined Computation, No Nacelle

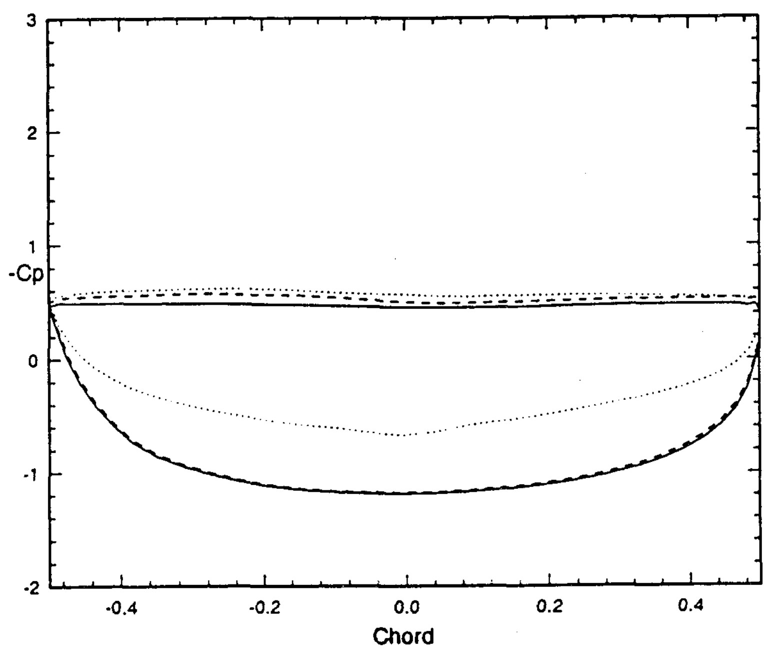

Figure 6. Pressure Distribution, Combined Computation, with Nacelle

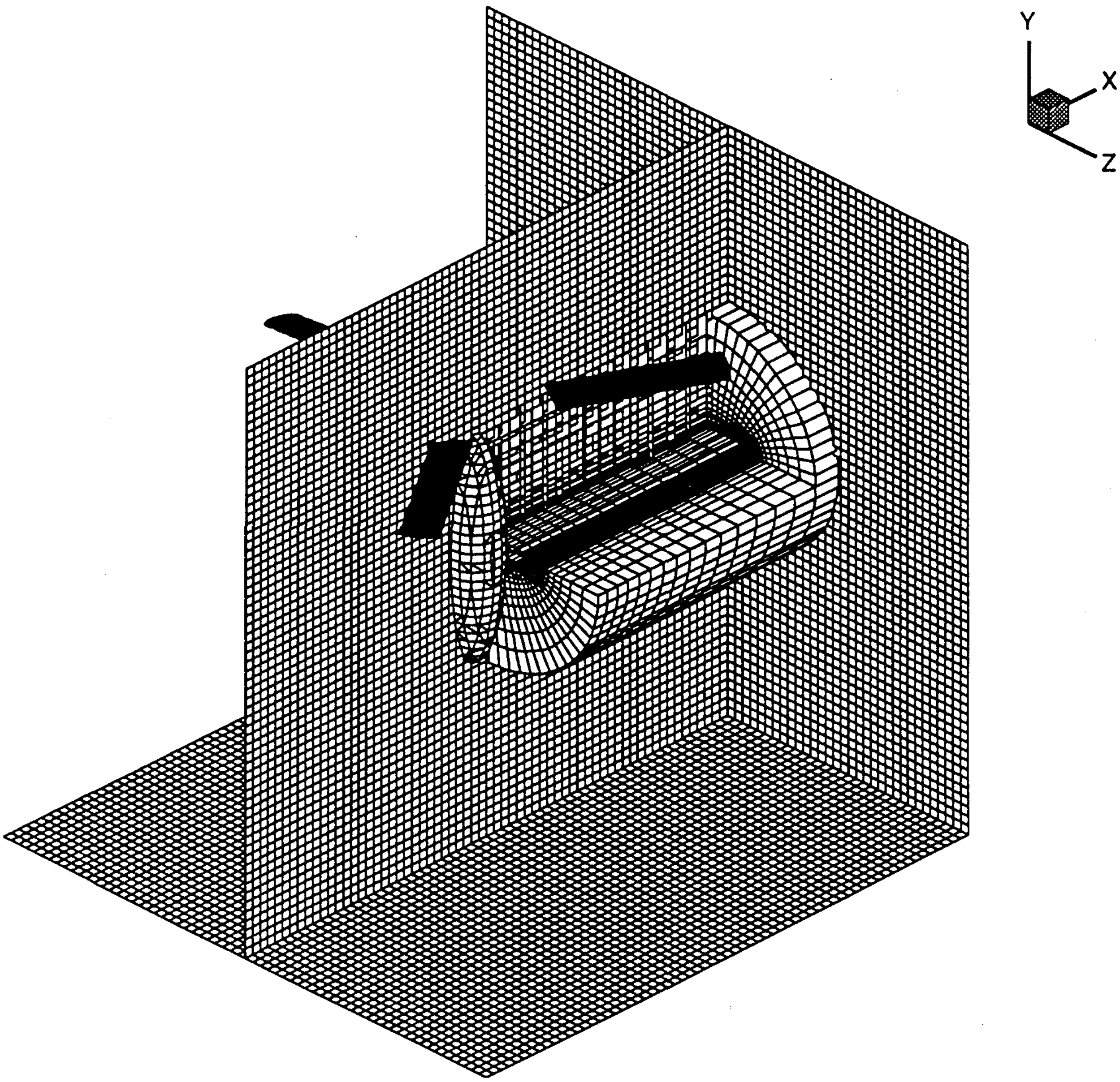

Figure 7. Uniform grid and a Body-Fitted Grid of the Wing

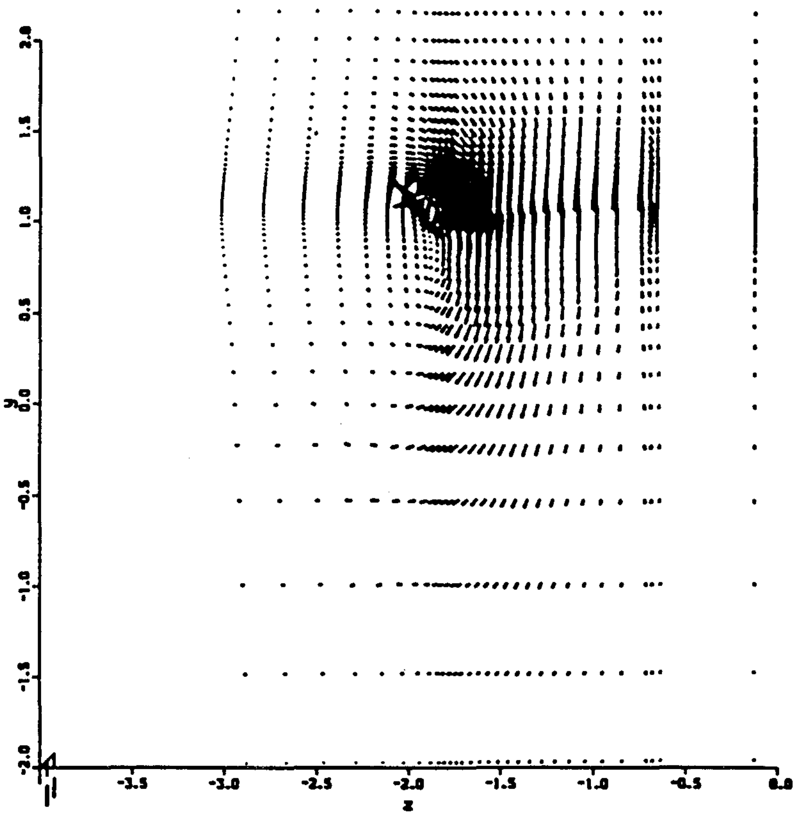

Figure 8. Velocity Field on a Plane Behind a Rotor Blade

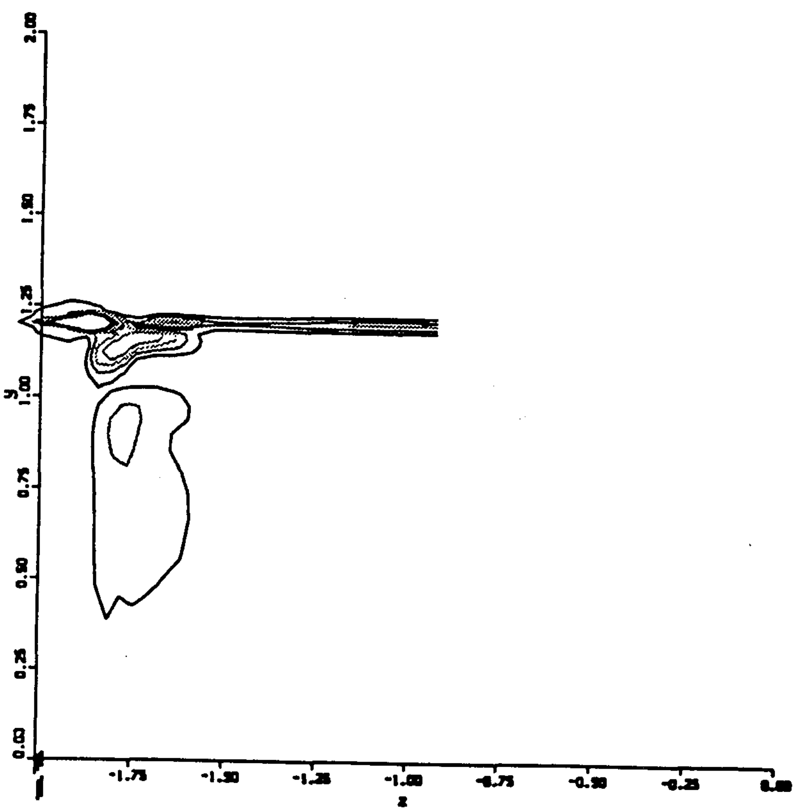

Figure 9. Vorticity Contours on a Plane Behind a Rotor Blade

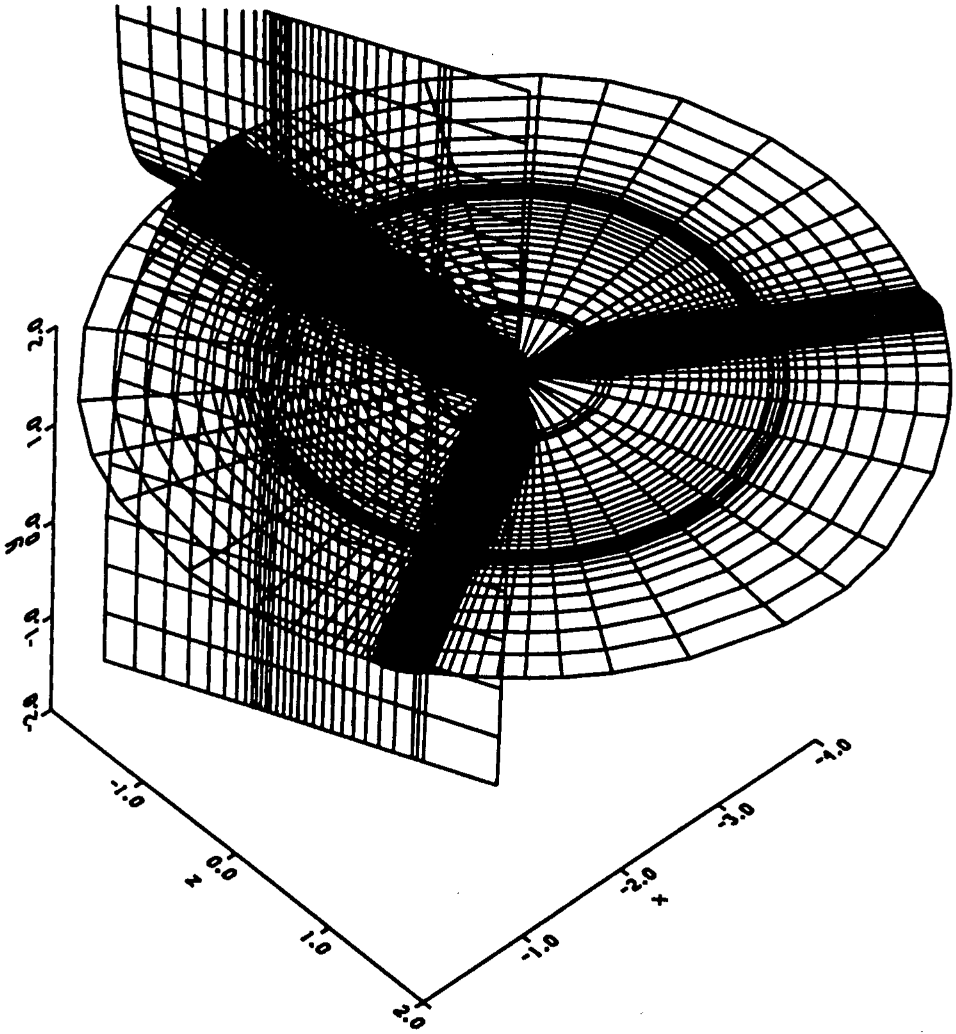

Figure 10. H-Grid used for HELIX Computation

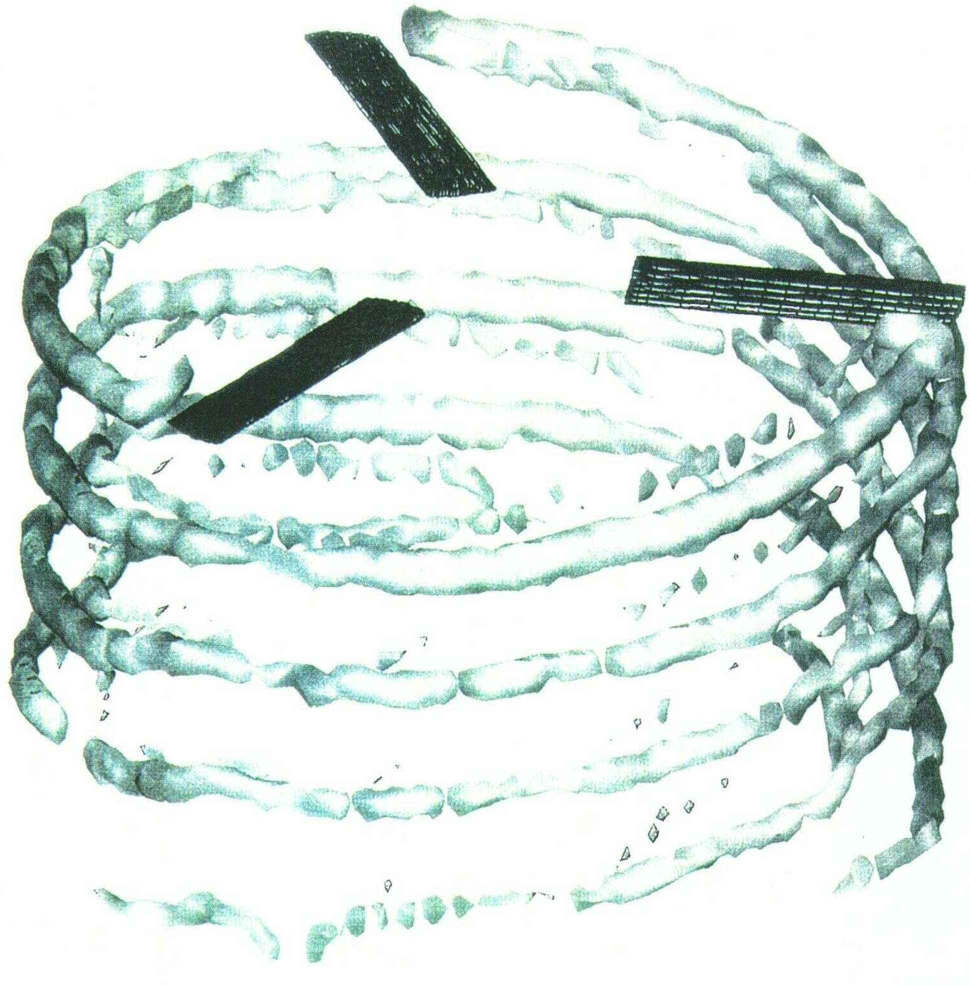

Figure 11. Wake Vortices of an Isolated Three-Blade Rotor

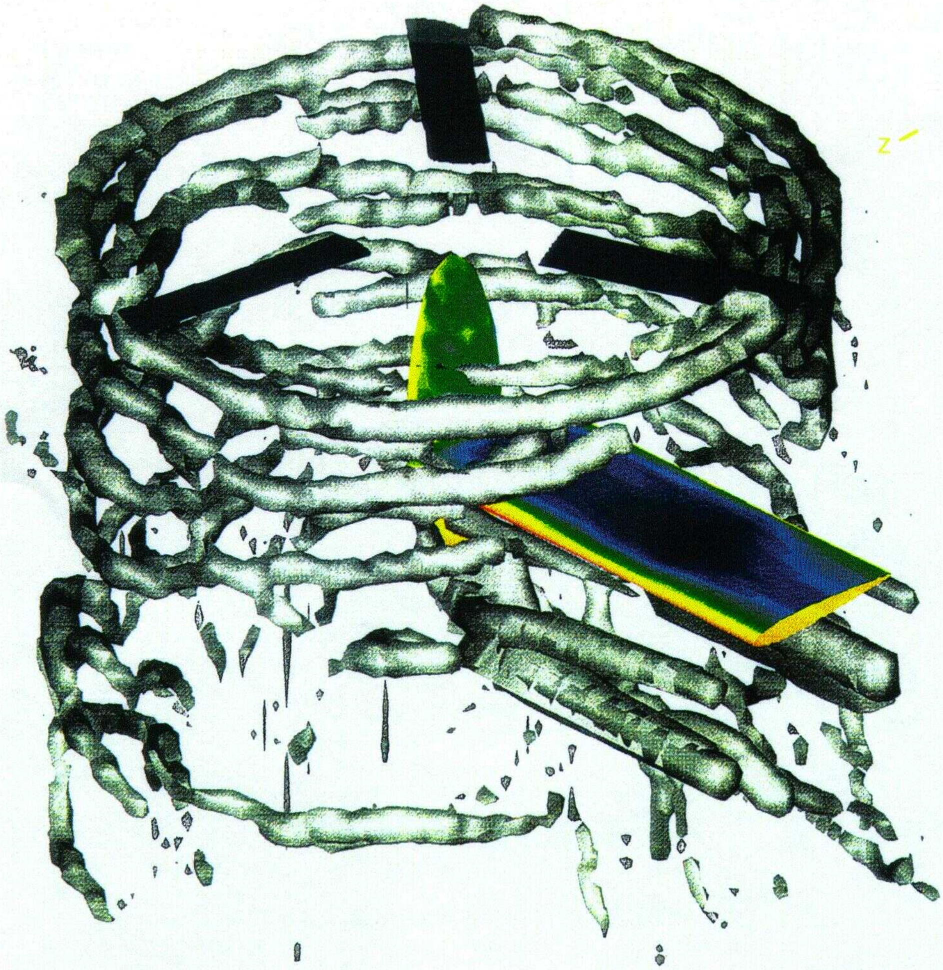

Figure 12. Wake Vortices of Wing-Nacelle-Rotor

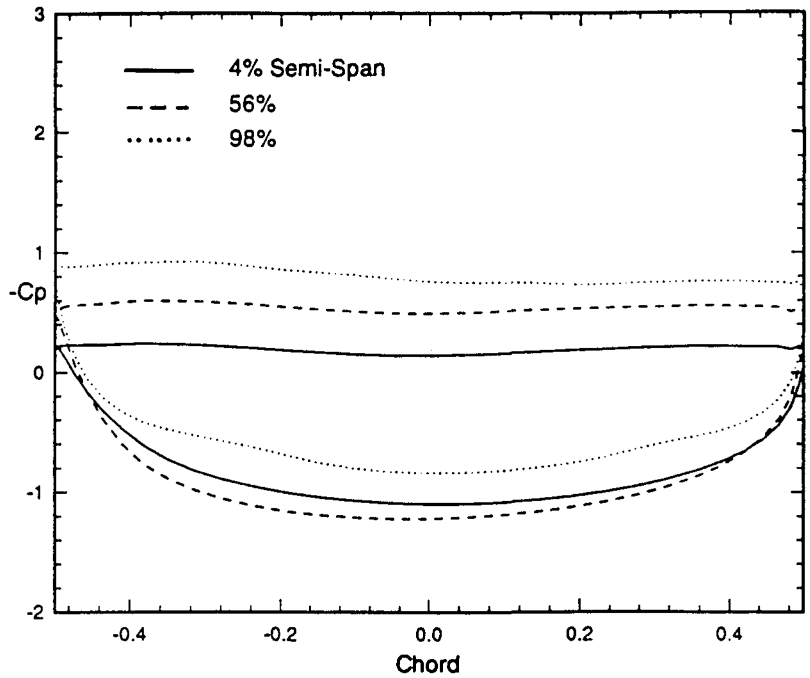

Figure 13. Pressure Distribution, with Nacelle and Rotor

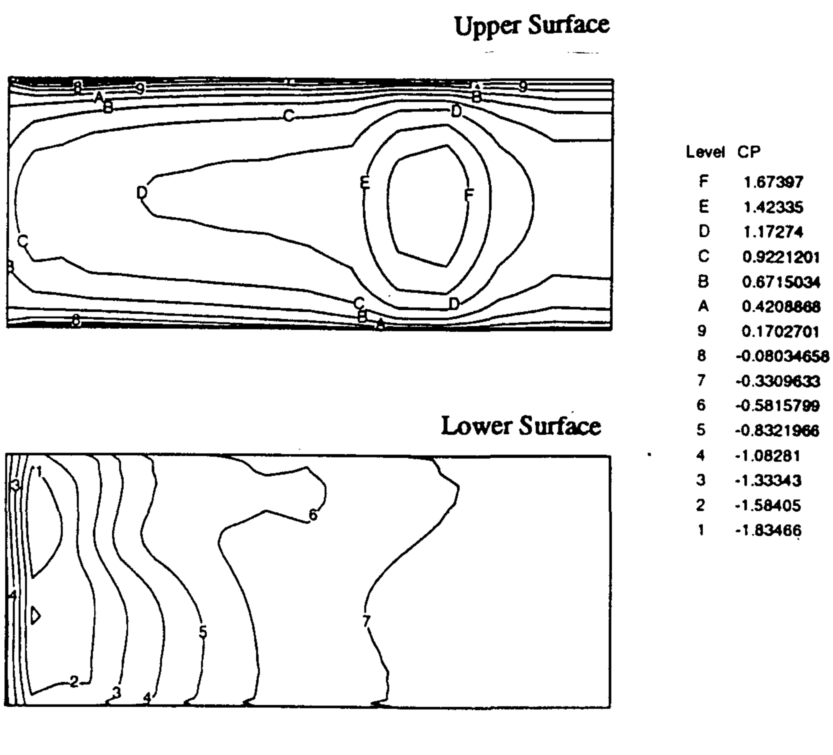

Figure 14. Pressure Contours, with Nacelle and Rotor